

A barium germanium 1,2-ethanediolato complex as precursor for barium metagermanate

Roberto Köferstein, Lothar Jäger, Mandy Zenkner, Hans-Peter Abicht*

Fachbereich Chemie, Martin-Luther-Universität Halle-Wittenberg, Kurt-Mothes Strasse 2, D-06120 Halle, Germany

Received 10 January 2007; received in revised form 23 February 2007; accepted 27 February 2007

Available online 2 March 2007

Abstract

The thermal behaviour of $[\text{Ba}(\text{HOC}_2\text{H}_4\text{OH})_2\text{Ge}(\text{OC}_2\text{H}_4\text{O})_3]$ (**2**) as a BaGeO_3 precursor, and its phase evolution during thermal decomposition in different atmospheres are described herein. The precursor complex decomposes in air to a finely divided mixture of BaCO_3 and GeO_2 , which subsequently reacts above 650°C to orthorhombic BaGeO_3 , transforming above 800°C to hexagonal BaGeO_3 . The shrinkage behaviour of BaGeO_3 compacts made from the as-prepared powders as well as from conventional mixed-oxide powders has been investigated. The samples were characterised by Fourier transformed infrared spectroscopy (FT-IR), X-ray powder diffraction (XRD), dilatometric measurements and thermoanalytic investigations (TG/DTA).

© 2007 Elsevier B.V. All rights reserved.

Keywords: Barium metagermanate; 1,2-Ethanediolato complex of germanium; Thermal decomposition; Phase evolution; Ceramics; Shrinkage behaviour

1. Introduction

Germanates have found important applications in material science and technology due to their dielectric, optical as well as acoustic–optical properties [1–4]. $\text{M}^{\text{II}}\text{GeO}_3$ ceramics with divalent metal ions such as Ba^{2+} , Sr^{2+} , Ca^{2+} , Ni^{2+} or Cu^{2+} are used on an industrial scale [5]. In particular, the addition of germanates, such as lead germanate, to barium titanate leads to a decrease in the sintering temperature and thus allows the production of heterophasic ceramic bodies of high electric strength and low dissipation factor [6]. BaGeO_3 exists in two polymorphic forms. Hexagonal (α)- BaGeO_3 (low-temperature form) has a pseudowollastonite-type structure in which the GeO_4 tetrahedra are linked to three-membered $[\text{Ge}_3\text{O}_9]$ -rings [7], whereas orthorhombic (β)- BaGeO_3 (high-temperature form) has a pyroxene-type structure, containing GeO_4 tetrahedra which are linked to two-periodic chains [8]. The phase diagram of the BaO – GeO_2 system was published by Guha [9] and shows the reversible hexagonal \rightleftharpoons orthorhombic transformation at 1200°C and a melting point at 1280°C . Moreover, Guha et al. [10] observed that the high-temperature form can

be retained at room temperature, depending on the cooling rate.

Usually, preparation of BaGeO_3 powder bases by the conventional mixed-oxide method, through the reaction of BaCO_3 with GeO_2 , requires temperatures of about 1100°C [10,11]. Yamaguchi et al. [12] briefly reported the simultaneous hydrolysis of a mixture of barium- and germanium alkoxides and subsequent decomposition to BaGeO_3 . The decomposition leads directly to the formation of orthorhombic BaGeO_3 below 1000°C . In Ref. [13] we reported the crystal structure of the precursor complex $[\text{Ba}(\text{HOC}_2\text{H}_4\text{OH})_2\text{Ge}(\text{OC}_2\text{H}_4\text{O})_3] \cdot 1.25 \text{HOC}_2\text{H}_4\text{OH}$ (**1**). This complex forms a ribbon-like polymeric structure. Briefly, Ba^{2+} is coordinated to nine oxygen atoms stemming from 1,2-ethanediol molecules, whereas Ge^{4+} is coordinated to three 1,2-ethanediol anions (c.n.=6). The oxygen atoms of the ligands also act as bridging atoms between the coordination polyhedra. As a result of the bridging function, rings are formed containing two $[\text{Ba}(\text{HOC}_2\text{H}_4\text{OH})_2\text{Ge}(\text{OC}_2\text{H}_4\text{O})_3]$ units. These rings are also bridged by 1,2-ethanediol molecules forming infinite ribbons. Uncoordinated 1,2-ethanediol molecules are situated between the ribbons. Even below 1000°C decomposition of **1** to BaGeO_3 occurs. Because of the relatively low calcination temperature this method supplies preceramic powders with higher sintering activity than powders fabricated by the mixed-oxide method. We are interested in the use

* Corresponding author. Tel.: +49 345 5525622; fax: +49 345 5527028.
E-mail address: hans-peter.abicht@chemie.uni-halle.de (H.-P. Abicht).

of BaGeO₃ as a sintering additive to reduce the sintering temperature for BaTiO₃ ceramics, with a view to producing nano-granular ceramics. The BaGeO₃–BaTiO₃ system, prepared by the conventional mixed-oxide method, was studied only by Guha and Kolar [14]. Here we describe in detail the phase evolution during thermal decomposition, in different atmospheres, of [Ba(HOC₂H₄OH)₂Ge(OC₂H₄O)₃] (**2**) yielding finally BaGeO₃. In addition, the shrinkage and sintering behaviour of powder compacts have also been investigated.

2. Experimental

2.1. Material preparation

In a previous paper we have described the preparation procedure for **1** and **2** starting from wet GeO₂·*n* H₂O with Ba(OH)₂·8H₂O in boiling 1,2-ethanediol [13]. However, in this work we used a modified method: germanium (IV) ethoxide (0.1 mol, Alfa Aesar GmbH & Co KG, Germany) and Ba(OH)₂·8H₂O (0.1 mol, Fluka Chemie GmbH, Switzerland) were dissolved in 1000 ml of boiling 1,2-ethanediol. After reflux for 24 h, 2/3 of the solvent was first removed under normal pressure and about 200 ml was then removed under reduced pressure at 100 °C. The reaction mixture was cooled and diluted with 100 ml of acetone. The resulting white crystalline precipitate of **2** was filtered off and washed with acetone (slow cooling also led to **1** in accordance with [13]). Yield: 65%.

Analysis: C₁₀H₂₄O₁₀BaGe (514.23 g/mol): calc. C, 23.36%; H, 4.70%, found C, 23.51%; H, 4.81%.

X-ray fluorescence analysis indicated a Ba/Ge atomic ratio of 1.007:1.

The phase evolution during the thermal decomposition of **2** was studied on samples which were heated up to 1050 °C (rate: 10 K/min) in a Pt-crucible in a static air or flowing oxygen atmosphere. The sample for shrinkage behaviour was calcined at 800 °C for 2 h in static air. In a teflon container, the resulting white powder (**2a**) was milled for 2 h using ZrO₂ balls in 2-propanol (*m*_{powder}:*m*_{balls} = 1:4). After filtering and drying the powder was mixed with 5 mass% of a saturated aqueous solution of polyvinyl alcohol as a pressing aid. The powder was pressed to discs with a green density of about 2.6 g/cm³. For comparative purposes, barium metagermanate powder (**3**) was also prepared by the conventional mixed-oxide method. For this preparation, BaCO₃ (Merck 1713, extra pure, Merck, Germany) and GeO₂ (99.998%, Sigma–Aldrich Chemie GmbH, Germany) were milled in a molar ratio of 1:1 for 24 h in a PVC container with the addition of distilled water and agate balls (*m*_{powder}:*m*_{balls}:*m*_{water} = 1:1:4). After filtering off and drying, the batch was calcined in static air at 1150 °C for 2 h to give a white powder. The remaining steps are identical to those mentioned above (as for **2a**). All observed crystalline phases were stable at room temperature.

2.2. Analytical methods

The infrared spectra were recorded on FTIR spectrometer Mattson 5000 (Mattson Instruments Inc., USA) at 25 °C in the

range of 350–4000 cm⁻¹ with a resolution of 2 cm⁻¹ as KBr pellets. X-ray powder diffraction (XRD) patterns were recorded by a STADI MP diffractometer (STOE, Germany) at 25 °C with the following equipment: transmission/Debye–Scherrer geometry, curved imaging plate detector, curved crystal germanium monochromator, Co Kα₁ radiation (1.78896 Å), and a step size of 0.03° for 2θ. Simultaneous thermogravimetric (TG) and differential thermoanalytic (DTA) measurements in different atmospheres were achieved using a STA 449C (Netzsch, Germany, Pt crucible, heating rate 10 K/min, flow rate 20 ml/min). The dilatometric investigations (shrinkage) were performed in a TMA 92-16.18 unit (Setaram, France, flowing air atmosphere, temperature rate 10 K/min and 5 min dwelling time at the highest temperature). The densities of the discs were calculated assuming an isotropic shrinkage behaviour. The specific surface area was measured using nitrogen three-point BET (Nova 1000, Quantachrome Corporation, USA). Measurements of the dielectric constants at 1 and 10 kHz were achieved using an Impedance Analyzer 4192 Alf (Hewlett Packard, USA) and a temperature rate of 0.5 K/min. An analyser CHNS 932 (LECO Instruments GmbH) was used for elemental analyses. Scanning electron microscope images were recorded with a Philips XL30 ESEM (environmental scanning electron microscope).

3. Results and discussion

3.1. Thermal behaviour of **2**

Figs. 1 and 2 show the TG and DTA curves up to 1000 °C for [Ba(HOC₂H₄OH)₂Ge(OC₂H₄O)₃] (**2**) in flowing air, oxygen and argon atmospheres, as well as under vacuum.

TG/DTA investigation in flowing air shows the beginning of an exothermic reaction at 157 °C. The corresponding weight loss of 22.8% differs a little from the calculated weight loss for two 1,2-ethanediol molecules per formula (24.2%). The loss of solvate molecules should be endothermic, but the loss of these 1,2-ethanediol molecules is accompanied by their decomposition. The splitting-off of the solvate molecules allows their decomposition to hydrocarbon fragments [15], which react with atmospheric oxygen to form CO₂ and H₂O on the surfaces of

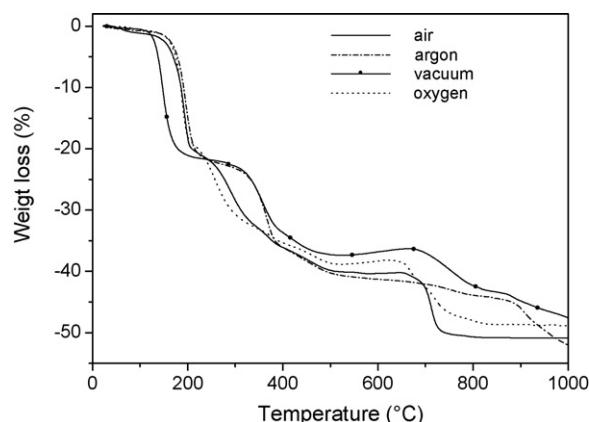


Fig. 1. TG curves of **2** in different atmospheres.

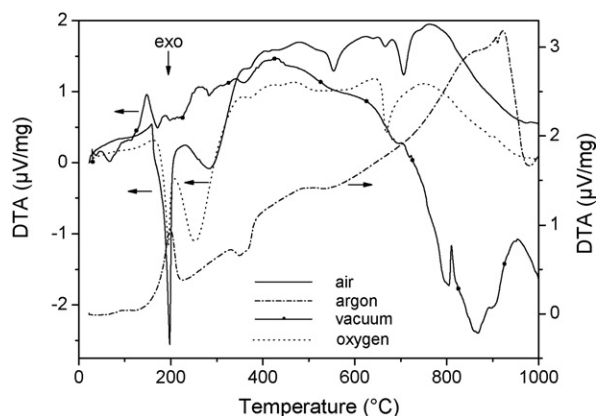


Fig. 2. DTA curves of **2** in different atmospheres.

particles. This exothermic reaction overlaps the endothermic one [16,17]. The desolvated compound is not stable. Several weight losses follow up to 564 °C leading to a total weight loss of 40.4%. Two exothermic peaks with onset temperatures of 232 and 479 °C can be observed. This state represents the complete transformation of **2** to a mixture of BaCO₃ and GeO₂ (calc. 41.3%). A two-step weight loss between 653 and 730 °C leads to the formation of BaGeO₃. During this process two exothermic peaks, with onset temperatures of 653 and 678 °C can be observed. The total weight loss amounts to 50.5% (calc. 49.8%). The XRD measurement of the final white product (1000 °C) indicates hexagonal BaGeO₃ and traces of Ba₂GeO₄ [18] (Fig. 3a). The transformation of **2** to BaGeO₃ is, with a heating rate of 1 K/min, complete at 700 °C.

The TG curve of **2** in an oxygen atmosphere is similar to the TG curve in air. They differ only in the final stage, which begins at 650 °C, leads to a gradual weight loss and is only finished at 827 °C. The total weight loss of 47.8% differs from the calculated value (49.8%). A XRD investigation shows that the final white product (1000 °C) consists of hexagonal BaGeO₃ and small amounts of Ba₂GeO₄ (Fig. 3b). However, the DTA investigation differs slightly from the investigation in air. The DTA curve shows two strong exothermic peaks with onset temperatures at 161 and 207 °C. Between about 340 and 520 °C two weak exothermic peaks can be observed. A final single strong exothermic peak appears at an onset temperature of 643 °C.

Unlike the behaviour observed in oxygen and air, the TG/DTA measurement under argon shows a broad endothermic peak between about 113–226 °C. The weight loss up to 264 °C is 22.4% and corresponds with the loss of the solvate molecules. This is followed by a gradual weight loss until about 501 °C and is consistent with the formation of BaCO₃ and GeO₂ (total weight loss 41.4%). A slight weight loss, starting at 717 °C, indicates the formation of orthorhombic BaGeO₃. The XRD diagram of a TG/DTA sample heated up to 850 °C (black coloured powder) mainly shows reflexions of orthorhombic BaGeO₃ and Ba₂GeO₄ (Fig. 3c). A final weight loss beginning at 876 °C, as a result of an endothermic process, continues up to 1000 °C to give a total weight loss of 52.0%. The final product at 1000 °C (grey coloured) consists of Ba₂GeO₄ and small amounts of orthorhombic BaGeO₃ (Fig. 3d). However, we cannot confirm any traces

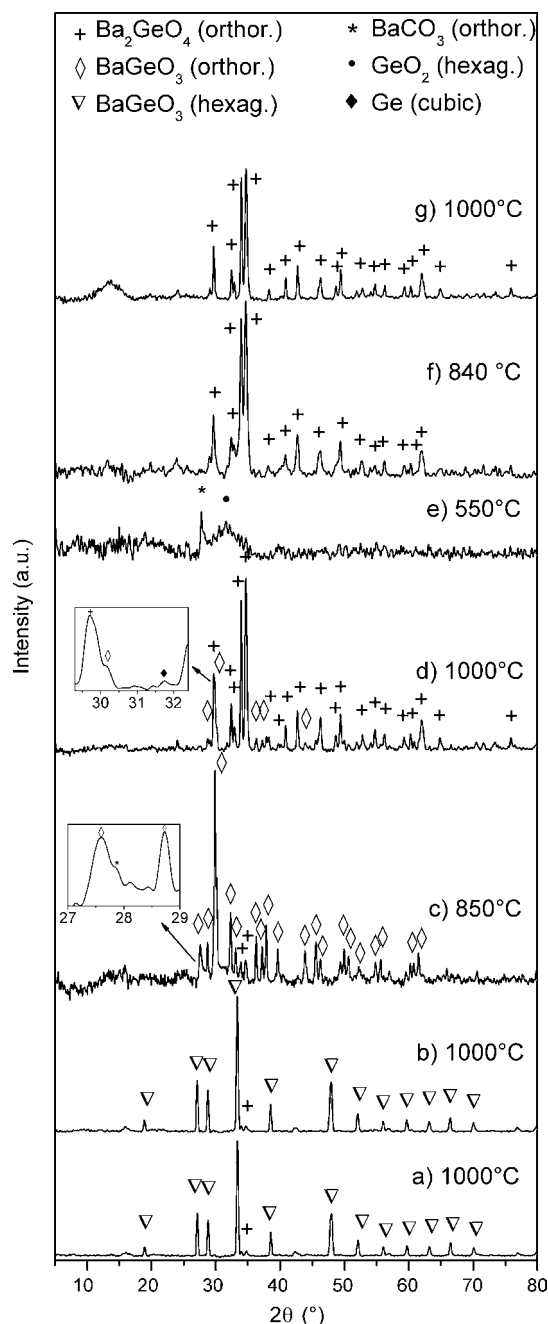


Fig. 3. XRD patterns of samples after TG/DTA investigations at the indicated temperatures in different atmospheres: (a) flowing air; (b) flowing oxygen; (c and d) flowing argon; (e–g) vacuum. The insets in (c) and (d) show an enlargement of the range between $2\theta = 27\text{--}32^\circ$ and $29\text{--}32^\circ$, respectively.

of BaGe₄O₉ formed by reaction of BaCO₃ and GeO₂ in a CO₂ atmosphere, as described by Kuno et al. [19]. The black-grey colour of the product arises from elemental carbon; an elemental analysis shows a carbon content of about 5 mass%. In contrast to the thermolysis in air and oxygen, **2** decomposes to BaCO₃ and GeO₂ reacting above 717 °C to form orthorhombic BaGeO₃ which decomposes to Ba₂GeO₄ with increasing temperature. The formation of Ba₂GeO₄ from BaGeO₃ is in principal possible in two ways. BaGeO₃ decomposes to Ba₂GeO₄ and GeO₂ (analogous to FeGeO₃ [20]) or to Ba₂GeO₄ and elemental Ge

under reducing conditions, as described by Royen et al. [21]. The exclusion of oxygen and the presence of elemental carbon can lead to reducing conditions at high temperatures. A very weak reflexion at $2\theta = 31.8^\circ$ in Fig. 3d possibly hints at the formation of small amounts of elemental Ge [18], but the signal-to-noise ratio is poor. Neither XRD nor IR investigations indicate the formation of other reduced compounds such as GeO [22]. The calculated weight loss of 52.9% for the formation of Ba_2GeO_4 and Ge differs only slightly from the observed value of 52.0%.

The DTA investigation under vacuum shows two endothermic peaks between 114–171 and 171–198 °C as well as a broad endothermic peak between 225 and 283 °C. These endothermic processes cause a weight loss of 22.1%. This is followed by a weight loss up to about 523 °C which leads to a very poor crystalline phase consisting of both orthorhombic BaCO_3 and hexagonal GeO_2 [18] (Fig. 3e). Between 679 and 1000 °C a two-step weight loss that results in a total weight loss of 47.6% is accompanied by two exothermic processes at 722–811 °C and 811–891 °C, respectively. The XRD diagrams of black coloured products at 840 and 1000 °C exclusively indicate reflexions of Ba_2GeO_4 (Fig. 3f and g). In contrast to the thermal behaviour under argon, Ba_2GeO_4 is formed directly by the reaction between BaCO_3 and GeO_2 .

The development of the specific surface area of **2** and its dependence on the calcination temperature is shown in Fig. 4. The small increase in specific surface area up to 200 °C suggests no major structural changes during the loss of the 1,2-ethanediol molecules. Further decomposition up to about 400 °C leads to an increase in specific surface area. The increasing specific surface area is not only caused by the evolution of consecutive gaseous products, but also by the different densities, and hence the molar volumes of **2** ($\rho \approx 2 \text{ g/cm}^3$) and the formed compounds BaCO_3 and GeO_2 ($\rho \approx 4 \text{ g/cm}^3$). The different densities lead to strains within the crystallites during the transformation, so that these crystallites collapse into a very large number of particles [23–25]. At about 600 °C the specific surface area fell to a minimum, although the TG curve in air shows several mass losses in this temperature range. The process of decomposition resulting in a larger specific surface area is compensated by

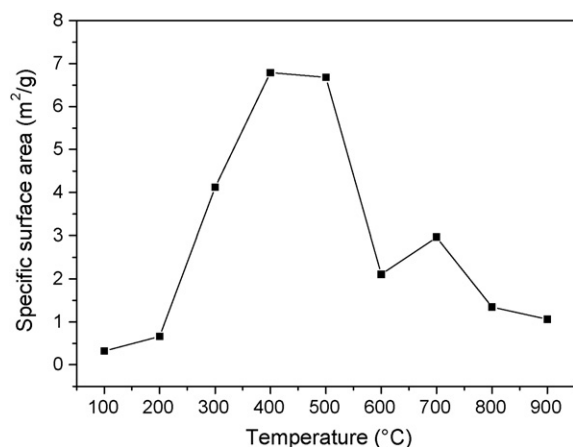


Fig. 4. Specific surface area vs. calcination temperature of **2** in static air (heating rate, 10 K/min; dwelling time, 1 h).

a sintering-like process (Ostwald ripening). A further increase in specific surface area between 600 and 700 °C is caused by the reaction between BaCO_3 and GeO_2 to form BaGeO_3 . As opposed to this behaviour, a decreasing specific surface area can be observed above 700 °C. The process between 700 and 900 °C corresponds to the Tammann number of $\alpha = 0.64$ – 0.75 , and therefore the sintering process can be explained as a lattice diffusion [26–28].

The particles of **2** exhibit a slab-like morphology (Fig. 5a). During the calcination process the resulting powders consist of slabs and broad staffs in different sizes (Fig. 5b). However, these particles show an additional microstructure consisting of globular grains, the grain size depending on the calcination tem-

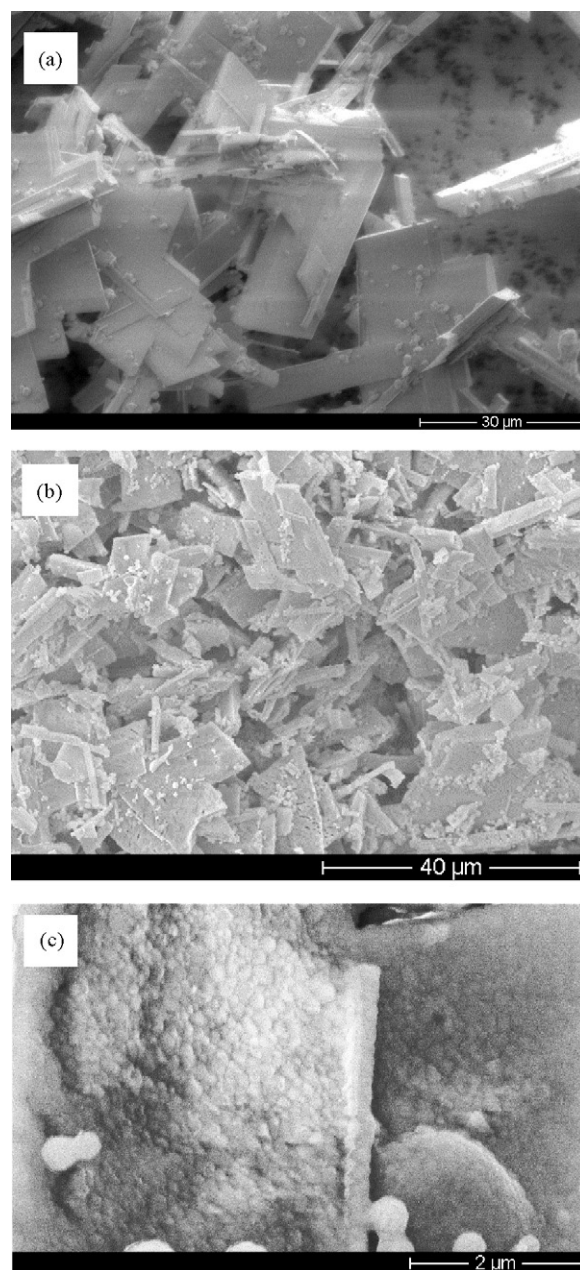


Fig. 5. SEM images of **2** (a) and calcined products (b) at 750 °C (1 h); (c) shows an enlargement of (a).

perature. A calcination temperature of 750 °C leads to a grain size of about 100–250 nm (Fig. 5c), whereas a temperature of 1000 °C leads to an enormous grain growth with grain sizes of about 1–3 μm.

3.2. X-ray powder diffraction (XRD) and IR spectroscopic investigation of **2**

The IR spectrum of **2** (Fig. 6a) reveals O–H stretching vibrations between about 3500–3000 cm⁻¹ and C–H stretching vibrations between 2950 and 2800 cm⁻¹ (not shown in Fig. 6). A broad peak at about 1645 cm⁻¹ is primarily due to water adsorbed by KBr. Between 1500 and 1200 cm⁻¹ absorption bands for CH₂ deformation vibrations can be observed (always coupled with a C–O–H deformation mode): 1459 cm⁻¹ (bending mode), 1344 cm⁻¹ (wagging mode), 1236 and 1212 cm⁻¹ (twisting modes, coupled with the wagging mode) [29–31]. The C–O stretching vibration is chiefly observed as a strong band at 1063 cm⁻¹ with a shoulder at 1088 cm⁻¹. The band at 902 cm⁻¹ with a weak shoulder at 877 cm⁻¹ (inset in Fig. 6b) is assigned to the CH₂ rocking mode [29,31]. Normal-coordinate calculations have suggested mode mixing among the C–O-, C–C stretching and CH₂ rocking vibrations in the gauche conformation of 1,2-ethanediol [32,33]. Therefore, the C–O stretching and

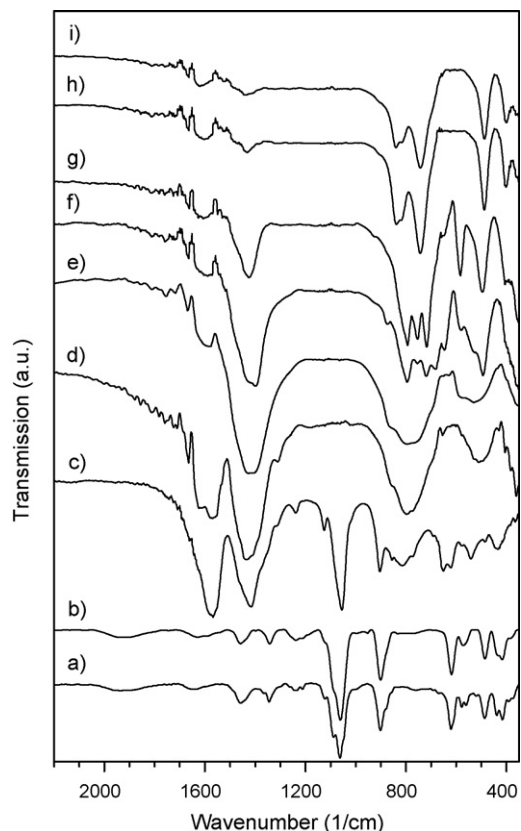


Fig. 6. IR spectra of **2** (a) and calcined products at various temperatures in static air (heating rate, 10 K/min; dwelling time, 1 h): (b) 200 °C, (c) 300 °C, (d) 400 °C, (e) 600 °C, (f) 700 °C, (g) 800 °C, (h) 900 °C, and (i) 1000 °C. Spectra e–i show a weak broad band at about 1600–1670 cm⁻¹ (δ_{OH}) due to water adsorbed by the KBr powder and the samples.

CH₂ rocking bands indicate that the 1,2-ethanediol molecules and 1,2-ethanediolate anions form a gauche-like conformation [34]. A comparison with **1** [13] supports this conclusion. Ge–O vibrations are mainly manifested at 621, 579, 487 and 417 cm⁻¹ (typical of GeO₆ octahedrons [35–37]).

The XRD pattern of **2** (Fig. 7a) shows a well-developed crystalline state of the powder in accordance with the results in [13].

3.3. Phase evolution during the thermal decomposition of **2**

3.3.1. IR spectroscopy

The IR spectrum (Fig. 6) of a sample calcined at 200 °C does not show any changes in comparison with the IR spectrum of **2**. Calcining up to 300 °C reveals bands belonging to the barium germanium (IV) precursor, new bands at about 1420 and 856 cm⁻¹ announcing the formation of BaCO₃ and a strong band at 1566 cm⁻¹, which probably indicates the formation of carboxylate groups. A number of the alkoxide groups of the precursor are possibly oxidized to –COO⁻ groups during calcination. Heating up to 400 °C results in the disappearance of the band at 1057 cm⁻¹ and an increase in the broad BaCO₃ band. The appearance of a strong new peak at 1621 cm⁻¹ indicates the formation of bridging O–H groups, which can also be observed during the thermolysis of other metal alkoxides [38,39]. This band becomes weaker with increasing temperature. The formation of GeO₂ (GeO₄ tetrahedra) is indicated by broad bands at about 793–770 cm⁻¹ and 580 cm⁻¹ [37]. After calcination at 700 °C bands in the range of 800–490 cm⁻¹ indicate the initial formation of orthorhombic BaGeO₃. Calcination at 800 °C reveals the typical IR pattern for germanate with a pyroxene structure, and thus the formation of orthorhombic BaGeO₃ [40]. The bands were assigned as follows: GeOGe anti-symmetric stretching vibration (the oxygen atom is bridging between two GeO₄ tetrahedra) at 794 cm⁻¹ and –OGeO⁻ anti-symmetric and symmetric stretching vibrations (the oxygen atoms are terminal ones of a GeO₄ tetrahedron) at 754 and 717 cm⁻¹, respectively. The appearance of two bands at 583 and 497 cm⁻¹, representing the GeOGe symmetric stretching modes, is characteristic of [Ge₂O₆]_∞ two-periodic chains [41,42]. The peak at 1425 cm⁻¹ represents the remaining BaCO₃. Heat treatment at 900 °C and higher for 1 h leads to typical infrared bands for hexagonal BaGeO₃ with the following assignments: anti-symmetric and symmetric –OGeO⁻ stretching modes at 841 cm⁻¹ (shoulder at 816 cm⁻¹), GeOGe stretching vibrations (ν_{as} and ν_{s}) at 743 and 488 cm⁻¹ and –OGeO⁻ in-plane rocking vibration at 401 cm⁻¹ [43]. The appearance of a band at 488 cm⁻¹ and the absence of the aforementioned peak at 583 cm⁻¹ is characteristic of the formation of a three-membered [Ge₃O₉]-ring [41,44].

3.3.2. XRD measurements

Phase evolution during the thermal decomposition of **2** was studied on samples by heating in a muffle furnace up to a certain temperature (rate 10 K/min), dwelling at this temperature and then cooling down to room temperature.

Fig. 7 shows XRD diagrams of samples heated up to 1000 °C in static air. Analogous to the IR investigations, it is only after

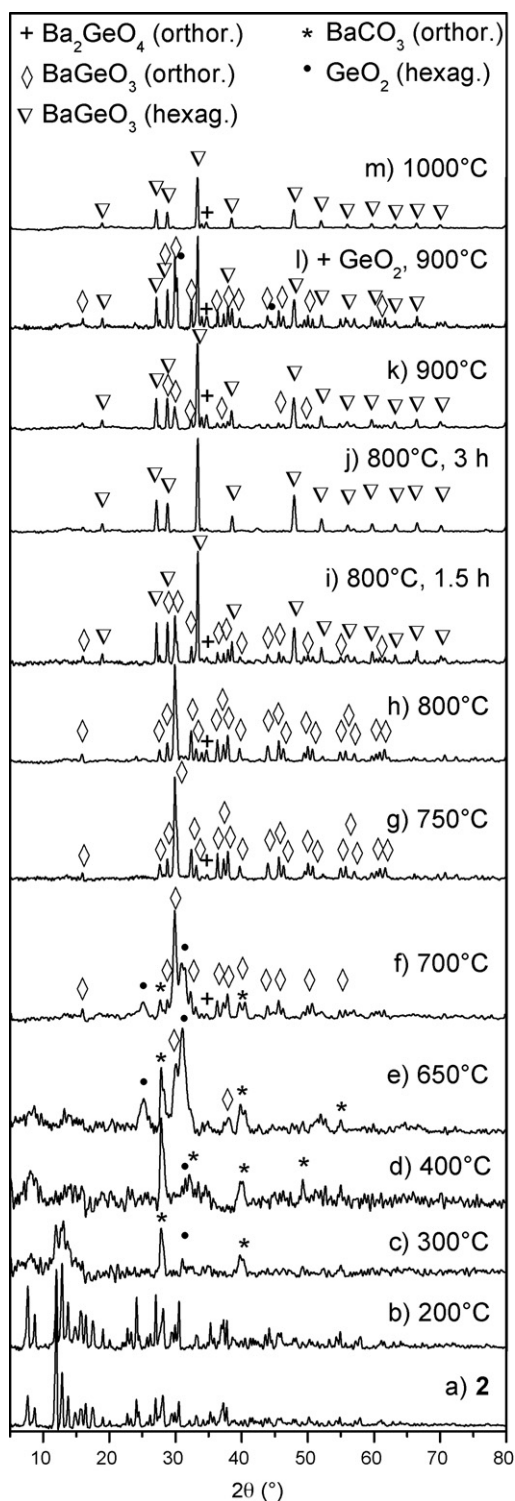
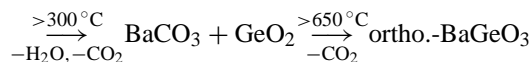
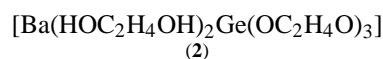


Fig. 7. XRD pattern of **2** (a) and calcined samples at the indicated temperatures in static air (heating rate, 10 K/min; dwelling time, 1 h, except pattern (i) 1.5 h and (j) 3 h). (l) Mixture of **2** and GeO₂ [83–543].

heat treatment to 300 °C for 1 h that decomposition of **2** appears to begin. The broad reflexions in the range up to $2\theta \approx 15^\circ$ can be assigned to residues of the precursor complex. The formation of BaCO₃ and hexagonal GeO₂ can also be observed. Only at a temperature of 400 °C does complete decomposition of **2**

to BaCO₃ and hexagonal GeO₂ occur. Orthorhombic BaGeO₃ appears above a calcination temperature of 650 °C. Elevation of the temperature to 700 °C results in an increase of orthorhombic BaGeO₃ content and a decrease in BaCO₃ and GeO₂, so that reflexions of BaCO₃ and GeO₂ disappear after a dwelling time of 10 h. Calcination at 800 °C for 1 h yields orthorhombic BaGeO₃. However an increase in the calcination time leads to the gradual formation of hexagonal BaGeO₃. We observed a complete transformation to hexagonal BaGeO₃ after more than 2 h. The XRD pattern of a sample calcined at 900 °C for 1 h shows the appearance of hexagonal BaGeO₃ with small amounts of orthorhombic BaGeO₃. Further heating to 1000 °C resulted only in reflexions of hexagonal BaGeO₃ and small traces of Ba₂GeO₄. The decomposition of **2** up to 1000 °C (dwelling time 1 h) in static air can be summarized as follows:



All samples calcined in static air between 300 and 700 °C showed a black-grey colour, ascribed to traces of elemental carbon. It can be seen that the thermolysis of **2** leads to orthorhombic BaGeO₃ at a low temperature, in contrast to the conventional synthesis [10]. Increasing calcination temperature (>750 °C) and time of exposure promoted the formation of hexagonal BaGeO₃. However, the infrared investigations show the presence of small amounts of unreacted BaCO₃ and consequently GeO₂ above 700 °C. It can be observed that a decrease in the unreacted species (especially GeO₂) leads to a gradual increase in hexagonal BaGeO₃. Heat treatment of a mixture of **2** with additional amounts of hexagonal GeO₂ [83–543] at 900 °C for 1 h clearly causes an increase in the orthorhombic BaGeO₃ phase (Fig. 7l). The appearance of orthorhombic BaGeO₃ below 1000 °C and its stability at room temperature is promoted by the presence of unreacted GeO₂ and small particle sizes. The dependence of the observed crystal structure on the particle size is also well known for BaTiO₃ and ZrO₂ [45,46].

Additionally, the formation of BaGeO₃ up to 1000 °C is accompanied by the formation of traces of Ba₂GeO₄. Only a heat treatment of at least 1050 °C for 2 h leads to pure BaGeO₃. Previous studies on a BaO–GeO₂ system by Zhmud et al. [47] and Jasim et al. [48] also described the presence of traces of Ba₂GeO₄. Analogous observations are reported for FeGeO₃ [49] and alkaline-earth metasilicates [50]. Fig. 8 shows XRD patterns for **2** at a calcination temperature of 750 °C and at different dwelling times. It can be seen, that the weak reflexions of Ba₂GeO₄ ((2 1 1), (0 2 0)) appear after the formation of orthorhombic BaGeO₃. After a calcination time of 1 min only reflexions of orthorhombic BaGeO₃ can be observed. A prolonged dwelling time of 30 min leads to the appearance of Ba₂GeO₄ reflexions. In contrast to the formation of BaGeO₃ from a conventional mixture of BaCO₃ and GeO₂ [21,49], we do not obtain a prior formation of Ba₂GeO₄ during the decom-

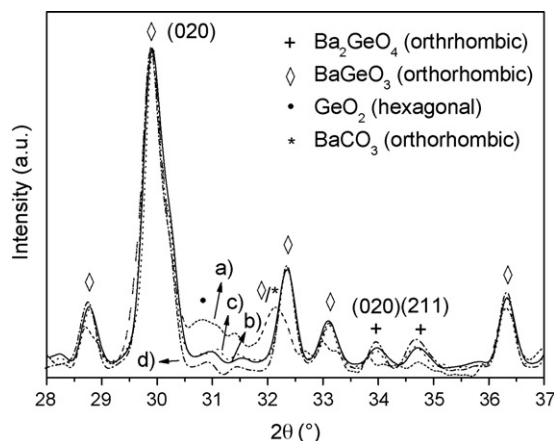


Fig. 8. Evolution of reflexions of BaGeO₃ and Ba₂GeO₄ through the decomposition of **2** at 750 °C in static air at different heating times. (a) 1 min, (b) 30 min, (c) 1 h, and (d) 10 h.

position of **2**. This means that **2** decomposes in air to yield a fine mixture of BaCO₃ and GeO₂, which reacts directly to BaGeO₃. Jasim et al. [48] reported that a portion of the BaGeO₃ possibly decomposed to Ba₂GeO₄ and GeO₂.

Thermal decomposition in a flowing oxygen atmosphere leads, at 300 °C, to the appearance of orthorhombic BaGeO₃ (Fig. 9). At a heating time of 5 min reflexions of Ba₂GeO₄ can be detected. Even a prolonged heating time leads only to a slight decrease of Ba₂GeO₄. Only an increased calcination tem-

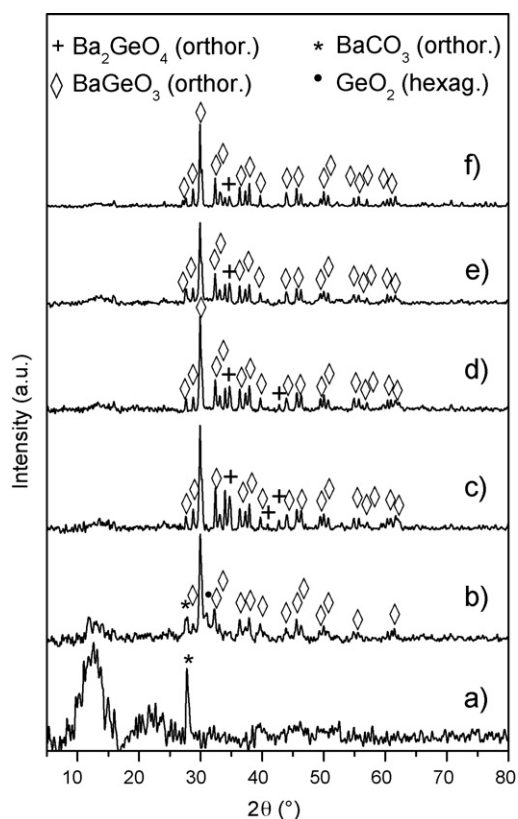


Fig. 9. XRD pattern of **2** calcined at various temperatures and dwelling times in flowing oxygen atmosphere (heating rate, 10 K/min): (a) 200 °C, 1 h, (b) 300 °C, 1 min, (c) 300 °C, 5 min, (d) 300 °C, 1 h, (e) 400 °C, 1 h, and (f) 800 °C, 1 h.

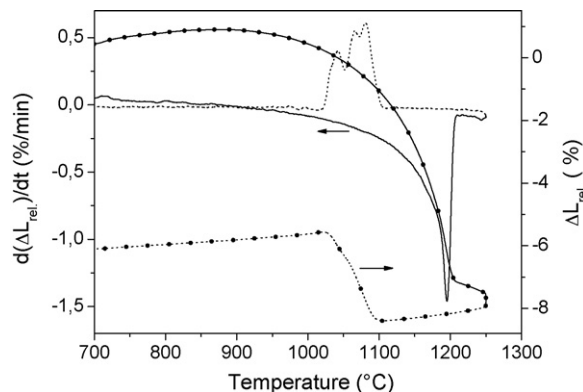


Fig. 10. The shrinkage behaviour up to 1250 °C of a green compact of BaGeO₃ (**3**). Solid lines represent the heating and dashed lines the cooling process.

perature reduces the Ba₂GeO₄ content. Under the conditions mentioned above, the decomposition in flowing oxygen takes place at a lower calcination temperature, but the resulting powders consist of hard agglomerates and contain higher amounts of Ba₂GeO₄ (up to 500 °C) in contrast to decomposition in static air.

3.4. Shrinkage and sintering behaviour

The preceramic powders, which were used for these investigations, consisted of hexagonal BaGeO₃. Fig. 10 shows the shrinking behaviour of a BaGeO₃ compact generated by the conventional mixed-oxide reaction (**3**) at 1150 °C for 2 h. The shrinkage starts at about 880 °C and the shrinkage rate reaches a maximum at 1195 °C. An increase in the shrinkage up to 1213 °C can be observed. Up to about 1200 °C a phase transition takes place from the hexagonal to the orthorhombic form [12,10]. At the end of the heating cycle, the relative density of the sintered body is 65% with reference to orthorhombic BaGeO₃. During the cooling cycle between 1096 and 1028 °C an expansion of the sintered body can be seen, which is caused by the reverse phase transition (orthorhombic → hexagonal), which is connected with a decrease in density on going from orthorhombic BaGeO₃ (5.16 g/cm³) to hexagonal BaGeO₃ (4.77 g/cm³) [7,8]. Moreover the expansion process is accompanied by a densification during the sintering process, therefore the expansion is about 4% and is lower than the expected value of 8%. The XRD pattern after the dilatometric measurement indicates hexagonal BaGeO₃.

The shrinkage behaviour of powder compacts, which were synthesised by the complex-precursor-method (**2a**) are shown in Fig. 11. The sample begins to shrink at about 805 °C and an increase in the rate of shrinkage is observed above 900 °C. The maximum shrinkage rate is reached at about 1174 °C. It is clear that, green bodies resulting from **2a** have a higher sintering activity than those of **3**. The enormous increase in the expansion of the sample during the cooling stage between 1100 and 1018 °C is due the reverse phase transition, as mentioned above. The better densification during the heating process up to 1250 °C yields the bodies with densities of 89% relative to orthorhombic BaGeO₃. Therefore, the reverse phase transition during the cooling phase

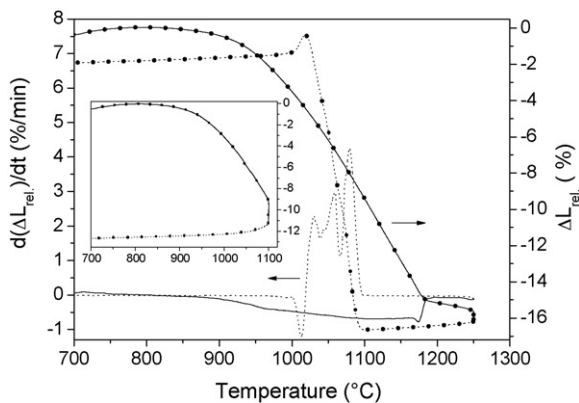


Fig. 11. The shrinkage behaviour up to 1250 °C of a green compact of BaGeO₃ (2a). The inset shows the dilatometric measurements up to a final temperature of 1100 °C. Solid lines represent the heating and dashed lines the cooling process.

causes high strains within the grain structure and leads to an extensive microcracking and finally to the destruction of the sintered body. Pure BaTiO₃ [51] and pure ZrO₂ [52,53] show an analogous behaviour. The crystalline phase detected after the cooling process was hexagonal BaGeO₃. However, heating up to only 1100 °C and cooling down to room temperature results in dense ceramic bodies, because no phase transition takes place in this temperature range (inset in Fig. 11).

The densities of ceramics after sintering at different temperatures (heating and cooling rate 10 K/min) are shown in Fig. 12. The bulk densities of the discs were determined by weighing and measuring dimensions. Green bodies of 3 require temperatures above 1200 °C to achieve comparable densities. Even sintering temperatures close to the melting point (1280 °C [9]) and a dwelling time of 10 h or longer leads to ceramics with a relative density of only 81%. Ceramics sintered below 1250 °C consist of hexagonal BaGeO₃ at room temperature. However, sintering temperatures ≥ 1250 °C and a dwelling time of more than 2 h hindered the reverse phase transition (orthorhombic \rightarrow hexagonal) during the cooling stage (independent of the cooling rate) and results in ceramics consisting of orthorhombic BaGeO₃. In con-

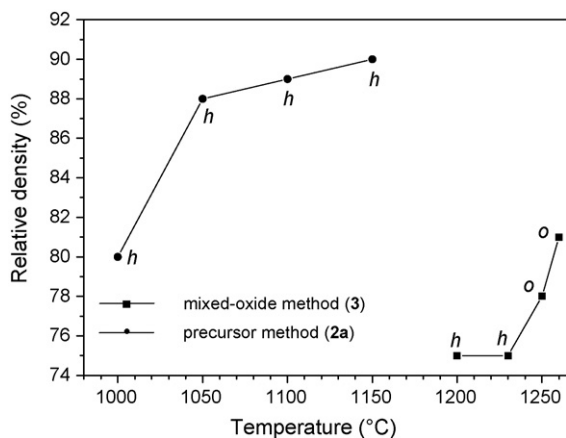


Fig. 12. Final density of sintered bodies depending on the sintering temperature. (a) Powder of 3 (sintering time 10 h). (b) Powder of 2a (sintering time 5 h). The relative density is related to the calculated X-ray density of the observed phase at room temperature; h = hexagonal phase, o = orthorhombic phase.

trast, green bodies of 2a show a better densification. The sintered bodies at 1000 °C (dwelling time 5 h) have a relative density of 80%. Up to a sintering temperature of 1150 °C ceramics with a relative density of 90% can be obtained.

Kher et al. [54] described an increase in the dielectric constant (relative permittivity, ϵ_r) between about 20–30 °C for BaGeO₃ prepared by the mixed-oxide method. Our dielectric measurements between 15 and 85 °C on ceramic discs formed by conventional mixed-oxide method, as well as by the precursor method, do not show any increase in the dielectric constant ($\epsilon_r \approx 17$). A possible reason for the anomalous behaviour reported by Kher et al. could have been the existence of impurities within the BaGeO₃ powder, since the authors described the used BaGeO₃ powder as a pinkish coloured powder.

4. Conclusion

The thermal decomposition of the [Ba(HOC₂H₄OH)₂Ge(OC₂H₄O)₃] (2) precursor in air proceeds to about 560 °C to yield a fine divided mixture of BaCO₃ and GeO₂, which subsequently reacts above 650 °C to afford BaGeO₃ and in contrast to the conventional reaction between BaCO₃ and GeO₂, without any evidence for a prior formation of Ba₂GeO₄. Furthermore, orthorhombic BaGeO₃ is observed below 900 °C. Decomposition up to 1000 °C under argon or vacuum leads to the formation of Ba₂GeO₄. The thermolysis of the precursor in static air leads to preceramic powders with clearly better sintering activity than conventionally produced powders. For this reason, the resulting ceramics show at a sintering temperature of no more than 1150 °C a relative density of 90%.

Acknowledgements

The authors thank Dr. Th. Müller for XRD, dilatometric and thermoanalytic measurements and for his helpful discussions and also Dr. U. Straube (Department of Physics) for the dielectric investigations. We are also grateful to Ms. M. Kelly for reading the manuscript. Financial support by the State Saxony Anhalt (Cluster of Excellence “Nanostructured Materials”) is gratefully acknowledged.

References

- [1] K. Sugii, H. Iwasaki, S. Miyzawa, *J. Cryst. Growth* 10 (1971) 127–132.
- [2] W. Taylor, T.J. Hosea, *Ferroelectrics* 25 (1980) 503–505.
- [3] H. Iwasaki, K. Sugii, T. Yamada, N. Nizeki, *Appl. Phys. Lett.* 18 (1971) 444–445.
- [4] H. Koelmans, C.M.C. Verhagen, *J. Electrochem. Soc.* 106 (8) (1959) 677–682.
- [5] O. Yoshiharu, S. Yoshinori, T. Noboru, I. Isao, Germanates of divalent metals as powder for piezoelectric and dielectric ceramics. J.P. Patent No. 58199717 (1983).
- [6] D.A. Payne, S.M. Park, *Heterophasic Ceramic Composition*. US Patent No. 4,218,723 (1980).
- [7] F. Liebau, *Neues Jahrb. Mineral.* 94 (1960) 1209–1222.
- [8] W. Hilmar, *Acta Cryst.* 15 (1962) 1101–1105.
- [9] J.P. Guha, *J. Mater. Sci.* 14 (1979) 1744–1748.
- [10] J.P. Guha, D. Kolar, A. Porenta, *J. Thermal. Anal.* 9 (1976) 37–41.
- [11] R.S. Roth, *Am. Mineral.* 40 (1955) 332.

- [12] O. Yamaguchi, M. Ki, T. Niimi, K. Shimizu, *Polyhedron* 2 (11) (1983) 1213–1216.
- [13] L. Jäger, V. Lorenz, C. Wagner, T. Müller, H.-P. Abicht, *Z. Kristallogr.* 220 (2005) 183–187.
- [14] J.P. Guha, D. Kolar, *J. Mater. Sci.* 7 (1972) 1192–1196.
- [15] H. Thoms, M. Epple, A. Reller, *Solid State Ionics* 101–103 (1997) 79–84.
- [16] L. Erdey, F. Paulik, *Acta Chim. Acad. Sci. Hung.* 7 (1955) 27–44.
- [17] L. Erdey, F. Paulik, G. Svehla, G. Liptay, *Z. Anal. Chem.* 182 (1961) 329–335.
- [18] PDF 2 (International Centre for Diffraction Data, Pennsylvania) BaCO₃ [5–378], GeO₂ [83–546_{hexagonal}], BaGeO₃ [30–127_{hexagonal}; 37–137_{orthorhombic}], Ba₂GeO₄ [39–1257], Ge [4–545_{cubic}].
- [19] H. Kuno, A. Suzuki, Y. Sugimura, T. Yamaguchi, *Funtai oyobi Funmatsu Yakin* 14 (1) (1967) 38–42.
- [20] P. Royen, W. Forweg, *Z. Anorg. Allg. Chem.* 326 (3/4) (1963) 113–126.
- [21] P. Royen, G. Wilhelmi, A. Kreher, *Naturwissenschaften* (1965) 390.
- [22] J.R.T. Johnson, I. Panas, *Chem. Phys.* 249 (1999) 273–303.
- [23] D. Dillmore, D. Nicholson, *J. Chem. Soc.* (1962) 960–965.
- [24] V.V. Subba Rao, R.V.G. Rao, A.B. Biswas, *J. Inorg. Nucl. Chem.* 28 (1966) 415–420.
- [25] S.J. Gregg, *J. Chem. Soc.* (1953) 3940–3944.
- [26] G. Tammann, A. Sworykin, *Z. Anorg. Allg. Chem.* 176 (1928) 46–48.
- [27] G.F. Hüttig, *Kolloid-Zeitschrift* 98 (1942) 263–286.
- [28] G.F. Hüttig, *Kolloid-Zeitschrift* 99 (1942) 262–277.
- [29] H. Günzler, H. Böck, *IR-Spektroskopie – Eine Einführung*, Verlag Chemie GmbH, Weinberg/Germany, 1975, pp. 154–157.
- [30] P. Buckley, P.A. Giguere, *Can. J. Chem.* 45 (1967) 397–407.
- [31] D. Knetsch, W.L. Groeneveld, *Inorg. Chim. Acta* 7 (1) (1973) 81–87.
- [32] H. Matsuura, T. Miyazawa, *Bull. Chem. Soc. Jpn.* 40 (1967) 85–94.
- [33] T. Takeuchi, M. Tasumi, *Chem. Phys.* 77 (1983) 21–34.
- [34] A. Miyake, *J. Am. Chem. Soc.* 82 (1960) 3040–3043.
- [35] D.K. Breitingner, T. Grütznier, H. Wick, O. Schimmer, H. Eschelbach, *J. Mol. Struct.* 408/409 (1997) 383–386.
- [36] P.A.W. Dean, D.F. Evans, R.F. Philips, *J. Chem. Soc. (A)* (1969) 363–366.
- [37] P. Tarte, A.E. Ringwood, *Nature* 201 (4921) (1964) 819.
- [38] H. Thoms, M. Epple, H. Viebrock, A. Reller, *J. Mater. Chem.* 5 (4) (1995) 589–594.
- [39] H. Thoms, M. Epple, A. Reller, *Thermochim. Acta* 3375 (1997) 195–200.
- [40] B.D. Saksena, *Trans. Faraday Soc.* 57 (1961) 242–258.
- [41] A.N. Lazarev, T.F. Tenisheva, R.G. Grebenschikov, *Dokl. Akad. Nauk SSSR* 140 (1961) 811–814.
- [42] I.S. Ignat'ev, A.N. Lazarev, *Izv. Nauk Akad. Neorg. Mater.* 8 (2) (1972) 280–284.
- [43] I.S. Ignat'ev, A.N. Lazarev, *Izv. Nauk Akad. Neorg. Mater.* 8 (2) (1972) 268–279.
- [44] J. Choisnet, A. Deschanvres, P. Tarte, *Spectrochim. Acta* 31A (1975) 1023–1034.
- [45] B.D. Begg, E.R. Vance, J. Nowotny, *J. Am. Ceram. Soc.* 77 (12) (1994) 3186–3192.
- [46] R.C. Garvie, *J. Phys. Chem.* 69 (4) (1965) 1238–1243.
- [47] E.S. Zhmud, A.B. Ivanova, A.A. Kotly, E.P. Ostapchenko, *Z. Neorg. Khim.* 7 (1962) 2581–2590.
- [48] F. Jasim, I. Jameel, *Thermochim. Acta* 115 (1987) 37–44.
- [49] P. Royen, W. Forweg, *Z. Anorg. Allg. Chem.* 326 (3/4) (1963) 113–126.
- [50] W. Jander, J. Wuhrer, *Z. Anorg. Allg. Chem.* 226 (3) (1936) 225–247.
- [51] T. Müller, H.-P. Abicht, *cfi/Ber. DKG* 77 (9) (2000) E26–E31.
- [52] P. Duwez, F. Odell, *J. Am. Ceram. Soc.* 33 (9) (1950) 274–283.
- [53] D.L. Porter, A.H. Heuer, *J. Am. Ceram. Soc.* 62 (5/6) (1979) 298–305.
- [54] V.G. Kher, Ba.A. Patki, D.A. Deshpande, *Curr. Sci. India* 44 (2) (1975) 46–47.